

# Real-time Human Eye Resolution Ray Tracing in Mixed Reality

Antti Peuhkurinen<sup>1</sup> and Tommi Mikkonen<sup>2</sup>

<sup>1</sup>*Varjo Ltd., Helsinki, Finland*

<sup>2</sup>*Department of Computer Science, University of Helsinki, Helsinki, Finland*

**Keywords:** Mixed Reality, Human Eye Resolution, Ray Tracing, Real-time Rendering.

**Abstract:** Mixed reality applications require natural visualizations. Ray tracing is one of the candidates for this purpose. Real-time ray tracing is slowly becoming a reality in consumer market mixed and virtual reality. This is happening due to development in display technologies and computer hardware. Some of these examples are foveated rendering enabled high resolution displays, like Varjo mixed reality headset, and parallel computing enablers, like GPUs getting ray tracing hardware acceleration enablers, such as for example Nvidia's RTX. Currently, the challenge in ray tracing is resource need especially in mixed reality where low latency is wanted and with human eye resolution where high resolution needs are obvious. In this paper, we design and implement a novel foveated ray tracing solution called Human Eye Resolution Ray Tracer (HERR) that achieves real-time frame rates in human eye resolution in mixed reality.

## 1 INTRODUCTION

In this paper, we evaluate implementation of a real-time ray tracer that works at human eye resolution in mixed reality. We especially want to test the feasibility of using only ray tracing technologies in visualizations, where scenes can include changes per frame and contain different types of 3D objects, like ones with abstract shapes and ones with more common triangulated data. Ray tracing is especially suitable for mixed reality visualization purposes because of realistic reflections and refraction are easy to be reproduced with the method. As the starting point of the implementation, we use well known ray tracing designs. Furthermore, to achieve real-time frame rates needed in the mixed reality, we have set a limit for scene complexity.

In more detail, we use polar space for ray generation to achieve smooth falloff of resolution and to introduce an option to recreate the structure for ray intersections per frame to enable possibility for scene changes. Our goal is to visualize simple scenes with real-time changes. We want to keep the scene dynamic and be able to alter the scene structure per frame basis. In addition, we want to support multiple object formats used simultaneously in the scene.

The main contributions of this paper are

1. Ray tracing on human eye resolution with global illumination in mixed reality is shown possible.

2. Dynamic ray count, ray count and generation per frame can be dynamically changed to keep the frame rate real-time.

The rest of this paper is structured as follows. In Section 2, we present background technologies that can be readily used when realizing the above vision. In Section 3, we present implementation that demonstrates the proposed approach. In Section 4, we perform some measurements regarding the implementation. In Section 5, we draw some final conclusions.

## 2 BACKGROUND

In this section, we present the necessary background for the paper. The topics addressed include human eye resolution and other characteristics (Subsection 2.1), 3D model acceleration structures (Subsection 2.2), lighting acceleration structures (Subsection 2.3), and the description of the headset used in our design (Subsection 2.4).

### 2.1 Human Eye Resolution and Characteristics

Human eye has special characteristics that have an effect to any perceived resolution. The resolution seen drops rapidly when moving away from the area where

eyes are focused to. As an example, a curve demonstrating the perceived resolution, proposed by Hunziker (Hunziker, 2006), is shown in Figure 1. This has stemmed a lot of research interest, and there are multiple papers from the topic of applying gaze direction and visual acuity curve to the rendering (Patney et al., 2016; Spjut et al., 2020; Tursun et al., 2019; Koskela et al., 2019; Stengel et al., 2016; Guenter et al., 2012; Meng et al., 2018).

With the above in mind, a rendering system can be designed so that the rendering quality is not as high at the peripheral area as it is at the area currently being looked at, without a human using the system noticing the difference. The resulting degrees of freedom, liberating us from uniform precision requirements, will play a key role in our design.

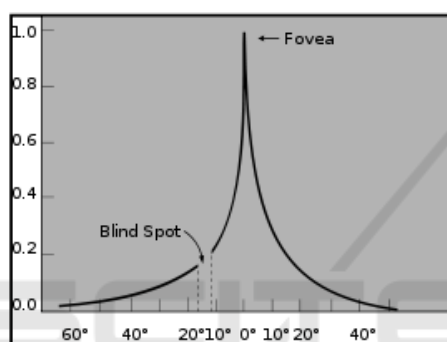


Figure 1: Visual acuity function of the human eye (Hunziker, 2006).

## 2.2 3D Model Acceleration Structures

For the ray intersection to be efficient the ray data and the object or bounding volume memory locality is important. This helps in the throughput of the system when intersections are being calculated in billions per second. Initial rays from user's eye are rather consistent. The reflection rays hitting the surfaces are nearly random. To ease these challenges, it is common to have a higher level data structure for the 3D data. A commonly used approach is a bounding volume hierarchy (BVH) presented by Kay and Kajiya (Kay and Kajiya, 1986).

A BVH can be used to define the up-most scene hierarchy with bounding volumes. Each object in the hierarchy is bounded with an axis-aligned bounding box (AABB) or with oriented bounding boxes (OBB) that can be optionally bounded by AABB. These bounding volumes can form a binary tree data structure, where each branch has a bounding box that is spanned over its children. BVH can have different degrees meaning how many children each node can have. Good examples from different degrees of BVH

is presented for example by Barringer (Barringer and Akenine-Möller, 2014).

### 2.2.1 Object Intersection

In the above setup, there are various ways rays can intersect objects within the volumes. Below we list the options we have considered as part of this research.

**Abstract Shapes.** Intersection of ray and simple abstract shapes, like AABBs, OBBs and spheres can be done few simple mathematical operations. For AABB ray intersection, there are several optimized algorithms, for example the one shown by Williams (Williams et al., 2005). OBB intersection is usually done by transforming the incoming ray to the OBB space and using then ray AABB intersection.

**Triangle Mesh Intersect.** Triangle intersection can use texture data for faster data access. In addition, complex triangle meshes can be split to multiple separate AABB blocks. Triangle data can be stored efficiently by using a single vertex and two edges being stored in a 1D float texture in a barycentric coordinate system (Möller and Trumbore, 1997).

**Voxel Intersect.** Voxels, meaning values on a regular grid, have many benefits in ray tracing over triangulated mesh used in rasterization. Voxel data structure can be also hierarchically mipmapped. This can be done for example averaging eight samples to one per each resolution step. This helps with the computational resource consumption, because lower resolution rays can be sampled using lower resolution voxel samples, therefore needing less deeper intersection walk into the octree (Williams, 1983; Meagher, 1980).

### 2.2.2 DirectX Raytracing

DirectX Raytracing (DXR) (DirectX Raytracing, 2018) enables two level hardware acceleration for ray intersections: for the ray to object intersection at the lower level, and ray to BVH intersection where BVH is created from the objects at the higher level. DXR uses term Top Level Acceleration Structures (TLAS) for the BVH structure and a term Bottom Level Acceleration Structures (BLAS) for the object level data. The object level data can be triangle based mesh data or custom data defined by the user. TLAS is formed from the set of bottom level data sets. High-Level Shading Language (HLSL) can be used for shader generation, hit, miss logic against the acceleration structures created.

### 2.3 Lighting Acceleration Structures

For lighting, we wanted to use classical ray tracing pattern where the first hit and reflection rays hit are being lit by ambient, diffuse, specular light. To create more realistic visuals, we are interested in soft shadows. The creation of soft shadows with area lights can be implemented by sampling the area light with multiple samples per intersection. With multiple samples, we can deduce what part of the area light is being occluded and what part is hitting the intersection.

In addition to soft and hard shadows done with direct lighting hits, we were interested from global illumination to achieve natural looking results. From the current research on global illumination the most suitable option for our case was to use probe based structure for the light bounces that reduces of amount of calculations needed to be done for example when compared to path tracing. There is a good research paper from the global illumination from Majercik et al. (Majercik et al., 2019) covering the 3D grid of probes being used for global illumination where single bounce per frame is calculated to achieve infinite bounces. They call the method as dynamic diffuse global illumination. This method has benefit of having limited and small performance hit but on the negative side it has lag. Earlier similar light capture has been described by Greger (Greger et al., 1998). In addition, short rays can be used for ambient occlusion to achieve more natural looking results.

### 2.4 Foveating Mixed Reality Headset

To research the ray tracing on human eye resolution we needed hardware that is capable to it. As our gadget in the experiments, we use the Varjo XR-1 headset (Varjo XR-1 Head Mounted Display, 2020). The headset is capable of running human eye resolution visuals using two different resolution areas. In total, the headset has interface with four viewports – two resolution areas for each eye. As visualized in Figure 2, the higher resolution area is available roughly 40 degrees field of view on x axis (FOVX) having 60 pixels-per-degree (PPD) and a lower one – 22 PPD – is 90 degrees. The headset has low-latency camera pipeline to achieve video see through effect. Gaze tracking follows the eye look-at upto single degree precision. The tracking system supported is Valve’s light beacon based system where device sensors are reading beams from the sensor for the position (Vive base station, 2020). In addition, an inertial measurement unit is integrated to the device for better orientation accuracy.

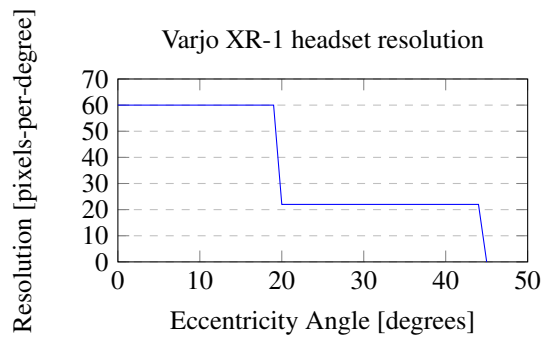


Figure 2: Varjo XR-1 headset resolution areas. High resolution area is used at the center of the FOV and blended to the low resolution area having larger FOV.

## 3 IMPLEMENTATION

The ray tracer implementation was custom-made to be used in research done in this paper. C++ was used for the scene loading as well as for data structure and object data creation on the CPU side. DXR APIs were used to implement the GPU side processing and rendering phases. Varjo software interfaces were used to draw to the headset displays and to read the device’s pose. Figure 3 presents an example still image from the headset view for the user.

Next we go through the implementation related topics. The topics include rendering pipeline (Subsection 3.1), managing dynamic resolution (Subsection 3.2), lights and materials (Subsection 3.3).

### 3.1 Rendering Pipeline

The rendering pipeline was designed to produce frames for the headset in real-time frame rates. Figure 4 presents the main phases used to create the frame for the displays. Below, the phases are discussed in more detail. We intentionally use rays for all main phases, like first hits, even if rasterization would most likely produce better results. The motivation is to have a simpler and uniform code base for future research.

When starting to create a frame, the most recent headset pose and gaze direction is read from the tracking systems and copied to the GPU side. Object data changes are applied to the GPU side memory. Any scene change – such as object or light pose change, new or deleted objects in scene etc – will invoke the update of the acceleration structures. Lighting structures are updated for every frame to achieve infinite bounces over time. This update means casting rays from probe, computing one bounce per frame more, and storing the information to probe’s texture. In addition, changes in object data, like new data or data



Figure 3: A still image from the left eye while rendering the test scene. For visualisation purposes a red circle for the eye direction is added. Notice the lower resolution far away from the eye direction. In addition, in the image the shadows from the virtual objects at the background can be seen at the floor and the statue is being lit also by the bounced light from the floor and the statue’s stand.

removal, lead to changes in the current GPU memory.

After we have all the latest information at the GPU side, we can start the actual rendering phases. Initially, we generate rays to the polar buffer where  $x$ -axis is the distance from the gaze direction and the  $y$ -axis angle counter clockwise from the camera right vector of the user’s gaze. A falloff mimicking the resolution of the human eye is applied as a part of this operation which be explained in detail at subchapter 3.2. After the rays are generated, we move to first intersections phase. We perform an intersection check with the BVH and its objects per ray. If a ray intersects an object, we generate lighting calculations needed for the global illumination. In this phase, we also store the addition a second intersection ray if the intersected material had reflection factor.

For the illumination, first light rays are being calculated from intersection point towards the light. If there are an area light and multiple light rays, the light ray targets are placed evenly over the target area light to generate information from the light amount hitting the intersection. The light rays will contribute to the color value, if they reach the light. We calculate the bouncing diffuse light from the probes by sampling the closest probes per hit and look with short rays the additional ambient occlusion effect.

The second intersection rays and light rays are calculated in a similar manner as the first ones.

To create the final buffer, we sample the polar buffer to create the four viewport buffers in Cartesian coordinates needed for the head mounted high and low resolution displays per eye.

This frame is then finally composited top of the video camera feed from the headset and shown to the user at the displays. The Varjo software system can warp the existing frame in low FPS scenarios to reorienting the existing frame, like post-rendering 3D warping addressed by Costella (Costella, 1993) and adding motion extrapolation similarly to Williams (Mark et al., 1997). This reorienting and adding of motion extrapolation is out of the scope of this paper.

### 3.2 Dynamic Resolution

To reduce computational resource usage we can create The visual acuity function can be used to define the pixel per degree value for a certain eccentricity angle (Hunziker, 2006; Koskela et al., 2019). For the resolution related to the angle, we found multiple different functions behaving adequately for our purposes. In the end, we decided to use the following function in our implementation that matches well to the the human eye resolution falloff and the display system in overall – we can alter still the amount of pixels used to render the frames to achieve dynamic resolution:

$$f(x) = 200/(x + 1), \quad (1)$$

where  $x$  is the eccentricity angle in degrees. The function produces good results and matches rather well to the human eye resolution falloff discussed earlier. We can use this function to define how we generate rays to polar coordinates. This function gives too many samples near the look-at area, but works well if the

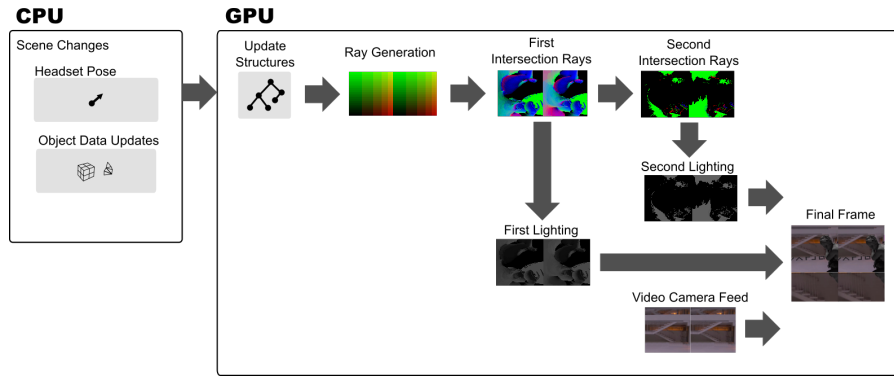


Figure 4: Rendering phases from scene changes to the final frame.

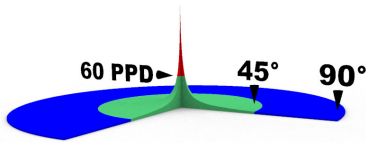


Figure 5: Visual acuity function visualized as 3D volume. Vertical axis is the PPD value and horizontal axis is the eccentricity angle. Base color for the volume is green. Volume over 60 PPD mark has red color. The volume over 45 degrees is colored as blue.

dynamic resolution is lowered and tackles well the tolerance and lag in eye tracking. Figure 5 demonstrates the resulting visual acuity falloff.

Next, we go through an example based on the above equation. Using integral from this function, we can see the resolution in radius dimension for the buffer. For example, when looking at the very center of displays then from 0 to 45 degrees the resolution need would be as follows:

$$f(x) = \int_0^{45.0} 200/(x+1)dx \approx 765.728$$

Then, the radius dimension needs at least 766 samples for 45 degree FOV to achieve resolution of the visual acuity function. Polar buffer texture location from current Cartesian buffer texture location can be calculated with the next equation:

$$x_{polar} = 200 * \ln(x_{Cartesian} + 1)$$

where  $x$  is the  $x$  location at the texture. The polar texture location can be turned to radius angle degrees  $\rho$  with next function:

$$\rho = e^{x_{polar}/200} - 1$$

To ensure square sampling of the scene with the rays, roughly similar height as width used is enough. Rays used per eye for 90 degree FOV human eye resolution can fit to 1024 x 1024 sized data structures. Figure 6 gives a sample from display buffers used by

the headset. In this image debug polar buffer coloring can be seen at the background.

To maintain the FPS rate high enough for comfortable viewing experience, we made the system to alter the resolution depending on headset pose changes. This was made by altering the used texture width. The used width can be changed per frame according to the needs.

### 3.3 Lights and Materials

For the lighting visual quality, we implemented switchable modes to support real-time frame rates with lower quality and to have better quality with the cost of frame rate. This feature provides possibility to have nice soft shadows when looking at something without large headset pose delta between the frames. The global illumination uses probes that store irradiance and the distance to geometry to textures. In all visualizations, materials have diffuse color, specular, and reflection factors in use. Moreover, area light has a color and a size in 3D. We use AABBs as the shape for area light sources.

### 3.4 Scene Setup

We made two main test scenes to test our implementation. In Figure 7 we have an image from our general test scene. This scene is opened in more detail in measurements chapter. In Figure 8 we have the visual quality scene that was used to understand the resolution curve, texture sizes, and the level of detail (LOD) levels during the implementation phase of the system.

## 4 MEASUREMENTS

The headset used at the measurements was Varjo XR-1. PC used to run the headset has a single Nvidia GeForce RTX 2080 Ti with NVidia 445.75 drivers,

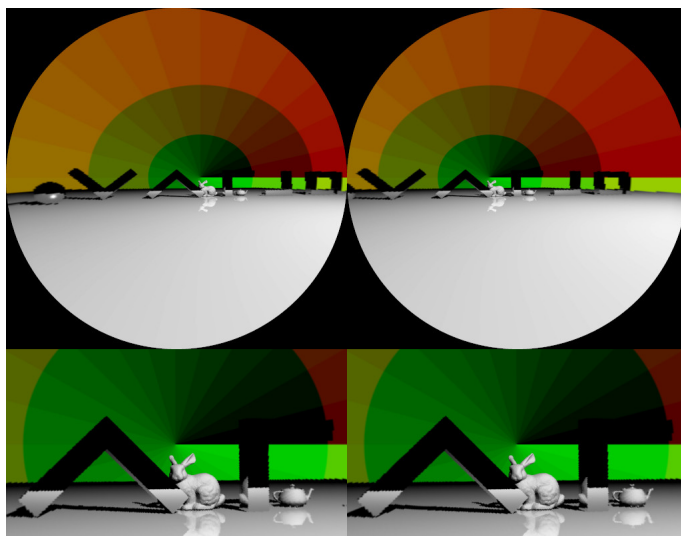


Figure 6: Sample image from the final frame buffer. Viewports showing the foveated rendering low resolution (at top) and high resolution (at bottom) buffers used for displays on a head mounted display. Background shows polar coordinate debug coloring having 15 degree tiles.

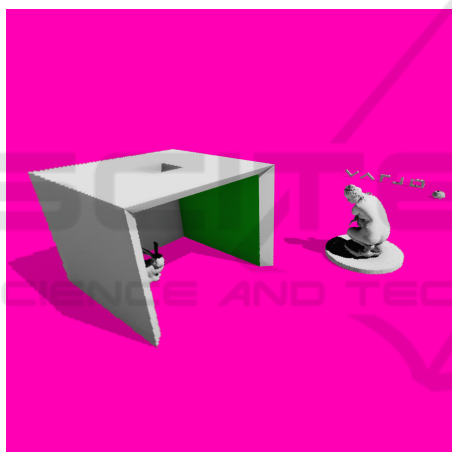


Figure 7: Mixed reality test scene used for the performance measurements. Picture is taken so that the camera can over-see the whole the scene. The pink color is used for visualization purposes for the mixed reality video see through area. The virtual shadows being cast and captured can be seen in the image as darkened areas. Test scene fits inside a 2.5 meters tall, 5 meters wide, and 10 meters long bounding box.

Intel i9-9960X @ 3.1 GHz CPU and Windows 10 operating system. In next subsections we go through the test scene used, the visual quality of different lighting settings and the frame creation times measured with different settings. It is important to note that we rendered full screen content and in mixed reality the rendered content is not usually filling the whole display area.



Figure 8: Test scene used to understand the resolution curve, the texture sizes, and LOD levels for models and their textures. When seated, the test images are filling the whole field of view.

#### 4.1 Test Setup

We used scene shown in Figure 7 to measure our solution. The scene has nine triangle based objects, in total having 290k polygons. All of these triangle based objects were static in our test scene. We used single area light for our measurements that was moving slowly in a circle path top of the objects. A grid of lighting probes was placed with even distances over the whole scene. Total amount of probes placed was 16 x 8 x 16, where 16 x 16 are on horizontal and 8 on vertical axis. Probes were placed with an even distance in the grid.

To experiment with the lighting, we had possibil-

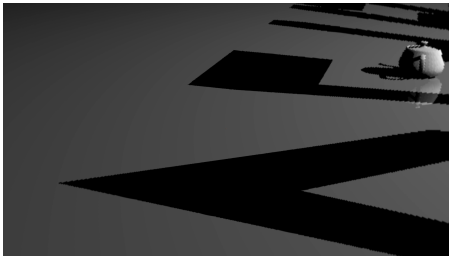


Figure 9: Single area light with 1 sample. Shadows are hard because single light sample is either hitting or being occluded.



Figure 10: Single area light with 64 light samples. The softer shadow can be easily seen when the shadow cast is further away from partially occluded light.

ity to change the amount of light samples being calculated. We ended up testing the scene with three different amount of samples per intersection. These options were next: the hard shadows with a single sample, soft shadows with 64 samples, and soft shadows with 256 samples. Figure 9 shows hard and Figure 10 soft shadows with 64 samples being used. The final frame buffer creation used bi-linear interpolation when sampling the polar buffer.

## 4.2 Frames per Second

To achieve real-time frame rates, the solution should be able to reach low frame creation times. Especially in virtual or mixed reality this is crucial to have for more pleasant experience. We measured the frame rates by taking an average over ten seconds in our test scene. We measured the frame-rates with different fixed resolutions to see the differences more clearly. In addition, we tested the lighting with two options: hard and soft shadows. We made test run with different amount of light samples per pixel to understand how complex lighting calculations can be. The frame rates were basically enough to have real-time graphics being drawn even with human eye resolution when low amount of lighting samples are used. With the more complex lighting setting the rendering speed was at interactive level only.

Table 1 presents the results measured from 10 second average with the different settings described

Table 1: Performance Measurements.

Average Frame Times				
Polar ray including eyes x polar samples]	buffer count [radius x polar pixel samples]	Frame time with 1 light sample per Pixel [ms]	Frame time with 64 light samples per pixel [ms]	Frame time with 256 light samples per pixel [ms]
1576 x 768		10.2	35.4	114.8
2048 x 1024		17.2	71.9	199.5

above. When not reaching the maxed out 60 FPS for Varjo's interfaces, the rendering speed was bounded by the ray intersection computations done at the GPU side. 790MB of GPU memory is used by the application. CPU load is under 5 percents and not affecting to the performance.

## 5 CONCLUSIONS

In this paper we have presented a ray tracer visualization for head mounted display with 90 degree field of view that can achieve human eye resolution and real-time frame rates. The results are encouraging because they show that it is possible to use ray tracing purely as the main visualization method – even with global illumination and scene updates being possible per frame.

Real-time rendering speed makes it possible to start consider more naturalistic visualizations especially in mixed reality situations, where the virtual and the real world are blended to each other. Examples from such effect are for example casting lighting and shadows from reality to another or reflecting or refracting lights between realities. These effects can be further enhanced with the real world environment information, like the shapes and materials.

Future work contains lighting and shadows related experiments to create more natural visuals between the realities. In addition, it would be also interesting to combine ray tracing rendering to our earlier research related to multiple simultaneously run mixed reality applications.

## ACKNOWLEDGEMENT

The authors thank the creators of next assets Utah Teapot (Martin Newell, 1975), Stanford Bunny (Marc Levoy, Greg Turk, 1994), Vase (Vase, Louvre Museum, 2016) and Aphrodite statue (Hoang Hiep Vu, 2015). These assets were found to be really useful during this research work. In addition, authors want

to thank Ville Miettinen from Varjo from tips related to the research work during its early days.

## REFERENCES

- Barringer, R. and Akenine-Möller, T. (2014). Dynamic ray stream traversal. *ACM Transactions on Graphics (TOG)*, 33(4):1–9.
- Costella, J. P. (1993). Motion extrapolation at the pixel level. *School of Physics, The University of Melbourne*.
- DirectX Raytracing (2018). <https://devblogs.microsoft.com/directx/announcing-microsoft-directx-raytracing/> Visited May 1, 2020.
- Greger, G., Shirley, P., Hubbard, P. M., and Greenberg, D. P. (1998). The irradiance volume. *IEEE Computer Graphics and Applications*, 18(2):32–43.
- Guenter, B., Finch, M., Drucker, S., Tan, D., and Snyder, J. (2012). Foveated 3d graphics. *ACM Transactions on Graphics (TOG)*, 31(6):1–10.
- Hoang Hiep Vu (2015). Aphrodite crouching. <https://sketchfab.com/3d-models/aphrodite-crouching-at-her-bath-better-854db6363e0b4957a93f8db4790510ec>, licensed under CC BY 4.0, Visited August 1, 2020.
- Hunziker, H.-W. (2006). Im auge des lesers: foveale und periphere wahrnehmung-vom buchstabieren zur lesefreude. *The Eye of the Reader: Foveal and Peripheral Perception-from Letter Recognition to the Joy of Reading*. Zurich: Transmedia.
- Kay, T. L. and Kajiyu, J. T. (1986). Ray tracing complex scenes. *ACM SIGGRAPH computer graphics*, 20(4):269–278.
- Koskela, M., Lotvonen, A., Mäkitalo, M., Kivi, P., Viitanen, T., and Jääskeläinen, P. (2019). Foveated real-time path tracing in visual-polar space.
- Majercik, Z., Guertin, J.-P., Nowrouzezahrai, D., and McGuire, M. (2019). Dynamic diffuse global illumination with ray-traced irradiance fields. *Journal of Computer Graphics Techniques Vol*, 8(2).
- Marc Levoy, Greg Turk (1994). Stanford Bunny, <http://graphics.stanford.edu/data/3Dscanrep/>, Visited May 1, 2020.
- Mark, W. R., McMillan, L., and Bishop, G. (1997). Post-rendering 3d warping. In *Proceedings of the 1997 symposium on Interactive 3D graphics*, pages 7–ff.
- Martin Newell (1975). Utah Teapot, [https://graphics.cs.utah.edu/history/utah\\_teapot.php](https://graphics.cs.utah.edu/history/utah_teapot.php), Visited May 1, 2020.
- Meagher, D. J. (1980). *Octree encoding: A new technique for the representation, manipulation and display of arbitrary 3-d objects by computer*. Technical report IPL-TR-80-111, Rensselaer Polytechnic Institute, Image Processing Laboratory, Troy, NY, USA.
- Meng, X., Du, R., Zwicker, M., and Varshney, A. (2018). Kernel foveated rendering. *Proceedings of the ACM on Computer Graphics and Interactive Techniques*, 1(1):1–20.
- Möller, T. and Trumbore, B. (1997). Fast, minimum storage ray-triangle intersection. *Journal of graphics tools*, 2(1):21–28.
- Patney, A., Salvi, M., Kim, J., Kaplanyan, A., Wyman, C., Benty, N., Luebke, D., and Lefohn, A. (2016). Towards foveated rendering for gaze-tracked virtual reality. *ACM Transactions on Graphics (TOG)*, 35(6):179.
- Spjut, J., Boudaoud, B., Kim, J., Greer, T., Albert, R., Stengel, M., Akşit, K., and Luebke, D. (2020). Toward standardized classification of foveated displays. *IEEE Transactions on Visualization and Computer Graphics*, 26(5):2126–2134.
- Stengel, M., Grogorick, S., Eisemann, M., and Magnor, M. (2016). Adaptive image-space sampling for gaze-contingent real-time rendering. In *Computer Graphics Forum*, volume 35, pages 129–139. Wiley Online Library.
- Tursun, O. T., Arabadzhyska-Koleva, E., Wernikowski, M., Mantiuk, R., Seidel, H.-P., Myszkowski, K., and Didyk, P. (2019). Luminance-contrast-aware foveated rendering. *ACM Transactions on Graphics (TOG)*, 38(4):1–14.
- Varjo XR-1 Head Mounted Display (2020). <http://www.varjo.com/> Visited May 1, 2020.
- Vase, Louvre Museum (2016). Benjamin Bardou, <https://sketchfab.com/3d-models/vase-louvre-museum-low-definition-660fb742a5ff4580862cf5f9eb690d92>, Visited August 1, 2020.
- Vive base station (2020). <https://www.vive.com/> Visited May 1, 2020.
- Williams, A., Barrus, S., Morley, R. K., and Shirley, P. (2005). An efficient and robust ray-box intersection algorithm. In *ACM SIGGRAPH 2005 Courses*.
- Williams, L. (1983). Pyramidal parametrics. In *Proceedings of the 10th annual conference on Computer graphics and interactive techniques*, pages 1–11.